Environmental Technology & Innovation 37 (2025) 103921

Contents lists available at ScienceDirect

Environmental Technology & Innovation

journal homepage: www.elsevier.com/locate/eti

Waste napkin biochar with high-performance designed for antibiotic rapidly removal

Yiping Jin [a,b], Zhongwen Zhou [a,b], Siji Chen [a,b,*], Chunjie Tian [b,c,*], Guang Chen [a,b]

[a] College of Life Sciences, Jilin Agricultural University, China
[b] Key Laboratory of Straw Biology and Utilization, the Ministry of Education, China
[c] College of Resources and Environment, Jilin Agricultural University, China

ARTICLE INFO

Keywords:
Waste napkin
Biochar
In-situ doping
Rapid removal
Antibiotic

ABSTRACT

In this work, domestic refuse waste napkin (WN) was used as raw material, modified by different dyes and prepared to N-doped biochars via carbonation and activation methods. The results showed that the addition of dyes not only optimized the physicochemical properties of biochars, but also greatly improved the adsorption performances. The specific surface areas of N-doped biochars (BWN-CR, BWN-CV, and BWN-MO) were increased by 5.95–26.6 % compared with that of undoped biochar (BWN, 2173.13 m^2/g), similarly, the content of nitrogen atoms in the modified biochars increased by 0.50–2.03 times. In the adsorption experiments using tetracycline hydrochloride as adsorption model, the adsorption capacities of all N-doped biochars (938.71–1159.05 mg/g) were greater than that of most adsorbents including BWN (861.33 mg/g). After 10 cycles of use, both all of the biochars can still maintain more than 65 % of the performance, indicating their stable regeneration ability. This work not only prepared a series of biochars that can be used to efficiently remove antibiotics from water, but more importantly provided a new strategy for the high-value utilization of WN and further released the application potential of secondary resources.

1. Introduction

Cleaner production is a concept of sustainable development aimed at minimizing waste of resources and environmental pollution. The development of new and advanced technologies for the use of waste or by-products in the production of high-performance functional materials is very meaningful to upgrade these secondary resources into high value-added products and address the environmental shortcomings caused by conventional disposal methods (Basta and Lotyf, 2023; Zhou et al., 2024). Agricultural waste, industrial waste, and household waste, as carbon-rich materials, have been widely concerned by researchers and used to develop a large number of functional biochar materials for environmental governance, new energy storage, carbon sequestration emission reduction, and soil governance, such as biochar adsorbents, biochar supercapacitors, biochar fertilizers and so on (Khedulkar et al., 2023, 2024; Yu et al., 2024).

Napkin is a kind of household paper that people contact more closely and use more frequently in the daily life, and has become an essential sanitary cleaning product in many people's lives. The 2023 annual report released by the China Paper Association pointed out

* Corresponding authors at: Key Laboratory of Straw Biology and Utilization, the Ministry of Education, China.
E-mail addresses: jinvslv@163.com (Y. Jin), zhouzhongwen000@163.com (Z. Zhou), sijichen@jlau.edu.cn (S. Chen), tiancj@iga.ac.cn (C. Tian), chg61@jlau.edu.cn (G. Chen).

https://doi.org/10.1016/j.eti.2024.103921
Received 21 September 2024; Received in revised form 7 November 2024; Accepted 26 November 2024
Available online 29 November 2024

that the annual consumption of household paper in China has exceeded 11 million tons, an increase of 4.15 %. To some extent, the main raw materials for the production of napkins are complex, mostly wood pulp, cotton pulp, straw pulp or waste paper and etc. For similar products, waste disposal is often recycled to make recycled pulp to produce new batches of paper towels (Man et al., 2019, 2020; Li et al., 2020). Due to the high cost of recycling, and the economic value of recycled paper products is not high, most people are still willing to choose to waste napkins together with kitchen waste or household waste incineration, landfill, not only caused environmental pollution, but also greatly waste this renewable biomass resources (Son et al., 2024; Farmanbordar et al., 2024; Wang et al., 2024). With the substantial growth of the demand for household paper, the corresponding production of napkin waste paper will only increase, and the environmental and economic pressure brought by it will become more and more large, then, to find a useful and efficient way to deal with this challenge is very important and meaningful.

Since most of the raw materials for the production of napkins are lignocellulosic biomass, waste napkins can also be regarded as lignocellulosic materials, and preparing them into functional biochar products is undoubtedly a feasible way to improve its added value. However, the biochar produced by conventional preparation technology has a small specific surface area and a small number and variety of active functional groups, which directly affects the performance of biochar products and thus limits its application (Fu et al., 2024; Wen et al., 2023.). Biochar is often subjected to secondary modifications, such as doping, modification, or composite functionalized heteroatoms, to improve its physical and chemical properties and performance (Su et al., 2024; Li et al., 2023). Heteroatoms can produce active sites such as point defects and effective functional groups by disrupting the electron cloud density and spin structure of sp^2 hybrid carbon, thus reducing the chemical inertia of carbon substrate, especially nitrogen, which can significantly regulate the electronic structure of the hexagonal honeycomb structure of carbon matrix, and thus improve the adsorption or energy storage performance of biochar (Zhu et al., 2024), the key to affect the efficiency of nitrogen doping is to find suitable substances with high nitrogen content and modify them by appropriate means.

In this study, waste napkin is used as raw materials to produce high-performance biochar that efficiently removes antibiotics from water. Specifically, different synthetic dyes with high nitrogen content were selected as nitrogen-doped modifications, including monoazo dyes methyl orange, diazo dyes Congo red, and triphenylmethane dyes crystal violet. The waste napkins were modified with synthetic dyes by adsorption and combination reaction, and then prepared into biochars with high nitrogen content by carbonation-activation. Finally, tetracycline hydrochloride was selected as the model to explore its adsorption properties, including adsorption kinetics, adsorption isotherm, adsorption thermodynamics, and etc. This work is not only to prepare a batch of biochars with excellent adsorption properties which could efficient removal of antibiotics in water, more importantly, the effects of different nitrogen doping substances on the modification of napkin waste paper were compared, and the possible mechanism of the biochar modification process and adsorption process were explored, so as to provide a new strategy for the conversion of other secondary resources with high added value.

2. Experimental details

2.1. Materials

Waste napkin (WN) was collected at breakfast joints in local markets. All chemicals include Methyl orange (MO, CAS: 547–58–0), Congo red (CR, CAS: 573–58–0), Crystal violet (CV, CAS: 548–62–9), tetracycline hydrochloride (TH, CAS: 64–75–5), sodium hydroxide (NaOH, CAS: 1310–73–2), and hydrochloric acid (HCl, CAS: 7647–01–0) were purchased from Aladdin Chemical and not further processed.

2.2. Experimental methods

2.2.1. N-doping modification methods

WN washed, dried at 80 ℃ to constant weight, and crushed until flocculent, set aside. Prepare dye solutions of different concentrations (0.01 mol/L, 0.05 mol/L, and 0.1 mol/L), and take out 100 mL each and place them in triangular flasks. Weigh 2.0 g of WN in a triangular flask containing 100 mL of dye solution, and place the reaction system in a constant temperature shaking table at 30 ℃ for 12 h at a rotating speed of 150 RPM. The modified WNs were extracted and washed with deionized water to remove the unattached dye solution, and then dried at constant temperature at 80 ℃ to constant weight. WN modified by different dyes is denoted as "WN-Dye-Concentration", for example, "WN-CR-0.005" represents WN modified with 100 mL of CR solution with the concentration of 0.05 mol/L.

2.2.2. Biochar preparation methods

The preparation of biochar is divided into two stages, including carbonization process and activation process, which are carried out in a horizontal tube furnace under nitrogen protection. The temperature of the carbonization process is 600 ℃, the carbonization time is 60 min, and the heating rate is 10 ℃/min. The activator used in the activation process is sodium hydroxide, specifically, 0.5 g of carbonized samples was fully ground with the activator at the ratio of 1:4, and the mixture was activated at 700 °C for 60 min. The reaction residue reduced to room temperature is then washed with deionized water and 0.1 mol/L hydrochloric acid solution to remove carbonates and excess activators until the pH is neutral. The obtained biochar samples were dried to constant weight in a constant temperature drying oven at 80 ℃ and stored in a drying dish for later use. Carbonization samples and biochar samples are named ass "CWN-Dye-Concentration" and "BWN-Dye-Concentration", for example, "CWN-CR-0.005" and "BWN-CR-0.005" represent carbonization samples and biochar samples obtained from WN-CR-0.005, respectively. The abbreviations WNs, CWNs, and BWNs

represent raw, carbonized, and biochar samples under different treatments. Details of the physicochemical characterization tests of the samples are provided as section S1 in Supporting Materials.

2.3. Adsorption experiment methods

2.3.1. Adsorption experiments

The batch adsorption experiment tests were performed in a constant temperature shaker with a rotational speed of 150 RPM, away from light. Specifically, the 10 mg biochar sample was weighed and poured into a triangle bottle containing antibiotic solution of different concentrations. A certain volume of liquid was measured with a pipette at a specific time point, and the supernatant was removed after separation by a 12000 RPM centrifuge. After the tested volume was fixed by deionized water, the antibiotic concentration in the solution was measured by ultraviolet spectrophotometer (Agilent Cary-300, USA). Biochar adsorption capacity (Q_e, mg/g) is calculated as follows:

$$Q_e = \frac{(C_0 - C_e) \times V}{m}$$

where the abbreviations C_0, C_e, V, and m represent initial concentration, the equilibrium concentrations of solutions, the volume of the solutions, and the mass of the biochar.

In order to investigate the effects of contact time (0–120 min), initial solution concentration (50–500 mg/L), temperature (283–323 K), and pH (3−11) on the adsorption process, different models (including adsorption kinetics, adsorption isotherms, and adsorption thermodynamics) were used to carry out fitting analysis on the experimental data. Details of the model formulas are shown

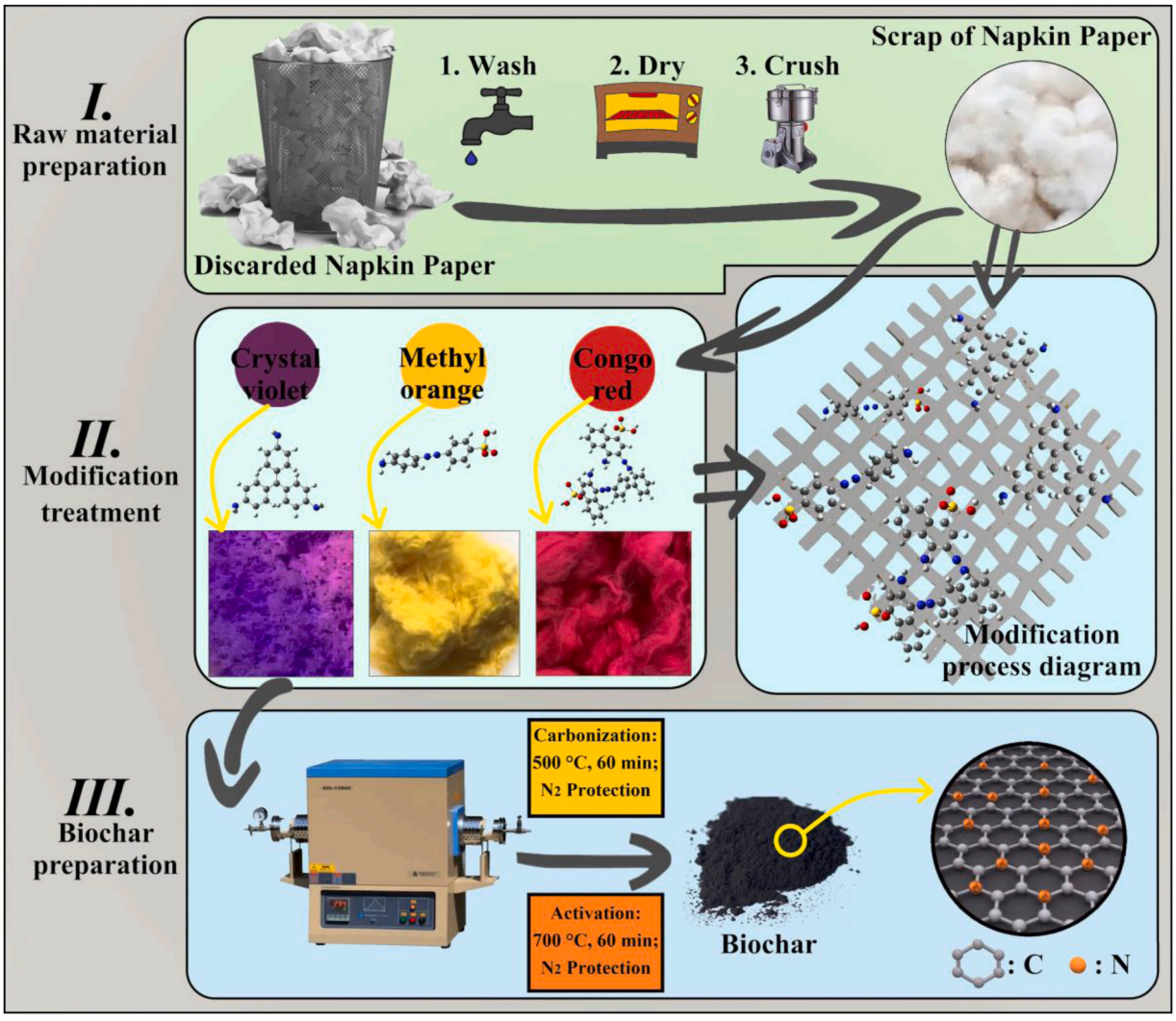

Fig. 1. Schematic of nitrogen-doped modification of waste napkin and preparation of derived biochars.

in section S2 of the Supporting Materials.

Cyclic adsorption tests were used to investigate the regenerative capacity of biochar, the details of which are shown in the S3 section of Supporting Materials.

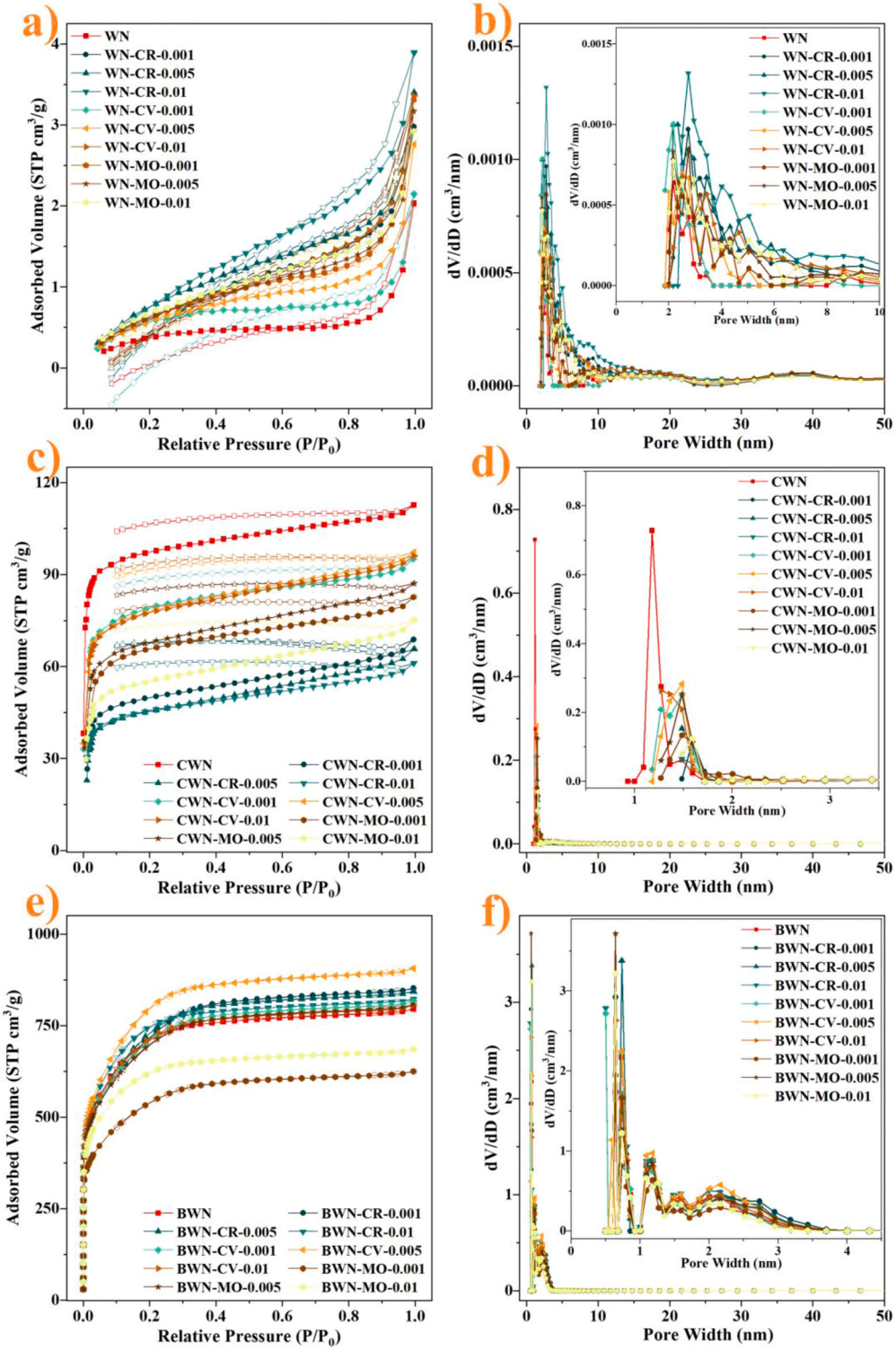

Fig. 2. (a) N_2 adsorption-desorption isotherms and (b) pore size distribution curves of WNs. (c) N_2 adsorption-desorption isotherms and (d) pore size distribution curves of CWNs. (e) N_2 adsorption-desorption isotherms and (f) pore size distribution curves of BWNs.

3. Result and discussion

3.1. Preparation of BWNs

The preparation process of BWNs is shown in Fig. 1. The collected WN is cleaned, dried and pulverized into flocculent paper scraps to increase its contact area with high nitrogen content substances, thus improving the successful efficiency of nitrogen doped modification. It is then evenly mixed with a solution containing CV, MO, and CR, and the doping process of nitrogen is completed by shaking in the flask. Generally speaking, the doping of different nitrogen-containing substances has different effects and possible mechanisms, similarly, the binding ways of the three high-nitrogen-containing substances and functional groups on WN surface are also different. CR is a typical diazo dye with molecular formula $C_{32}H_{22}N_6Na_2O_6S_2$ and 12.1 % nitrogen content, which is often used as an adsorption indicator, biological medium additive, and biological dye. It has been reported that it readily interacts significantly with polysaccharides containing continuous β-(1−4)-linked D-glucopyranosyl units, β-(1−3)-D-glucans, and some hemicellulose galactoseglucomannan (Teather and Wood, 1982). WN is also a typical kind of lignocellulosic material, therefore, it will also contain a lot of cellulose and hemicellulose, and can have a strong combination reaction with CR. CV is a typical triphenylmethane dye with molecular formula $C_{25}H_{30}N_3Cl$ and 10.3 % nitrogen content, which is widely used in cytology, histology, and bacteriology, and is an excellent staining agent. CV has a number of N and O ligands with strong alkalinity such as -NH_2 and -OH on each aromatic ring, which can combine with oxygen-containing acid ions on WN surface to form a relatively stable ion association by electrostatic attraction (Zarrik et al., 2024). MO is a mono azo dye. The molecular form is $C_{14}H_{14}N_3SO_3Na$ and 12.8 % nitrogen content, which is a commonly used acid-base titration indicator in analytical chemistry and is an important textile dye in the printing and dyeing industry. The structure of MO shows that it will expose an -NH_2 and a group containing -SO_3^{2-} on the molecular surface, which can interact with hydroxyl, carboxyl and other groups on the surface of WN, so as to bind together (Popat et al., 2024). Finally, BWNs containing nitrogen were prepared from modification treatment WNs by carbonation-activation process under nitrogen protection.

3.2. Characterization results

In order to explore the influence of nitrogen incorporation on the elemental composition of the samples and determine the concentration of the added dyes, EDS analysis was performed on all the samples, and the results were shown in Fig. S1 and Table S1. Specific analysis of C, O, and N elements in the samples showed that although N elements could be seen in the original sample spectrum, the content of N elements could not be accurately separated. This can be explained for two reasons. First, the EDS test is qualitative in nature, and the atomic number of the N element is small, so it is difficult to quantify accurately. Another reason is that the sample contains a large number of elements C and O, and the signal of the N element will partially overlap with it, so it is difficult to quantitatively analyze its composition. After carbonization, the signal of the three elements is enhanced, and the element composition in CWN is 90.8 % of C, 7.1 % of O, and 2.1 % of N. Because the raw material of WN is lignocellulosic material, although it has been treated by many processes in the paper forming process, there are still some residues of protein or amino acids, which are detected in CWN. With the incorporation of dyes, it can be clearly seen that the content of N element in CWNs has significantly increased. When the solution concentration is 0.005 mol/L, the N element content of CWN-CR-0.005, CWN-CV-0.005, and CWN-MO-0.005 were 3.8 %, 2.4 %, 2.3 %, respectively. With the further increase of the concentration, the content of N element did not further increase significantly, which may be due to the adsorption of WN and the chemical reaction of surface groups during the nitrogen doping process, that is, the capacity of WN itself to dye is limited. After activation treatment, the content of N element on the surface of BWNs, including BWN, has a slightly decreasing trend, which may be caused by the etching of carbon precursors by activators during the activation process. Specifically, the activator is partially combined with the carbon precursor in the process of high-temperature activation to form carbonate substances, which are removed by later cleaning, and the carbon precursor mixed with nitrogen element will also be affected in the same process.

The specific surface area and pore structure of a biochar material are among the key indicators used to assess its physical and chemical properties (Yang et al., 2023). In addition, in order to optimize the concentration of nitrogenous substances during the modification process, samples prepared under all conditions, including WNs, CWNs and BWNs, were tested by low temperature nitrogen adsorption-desorption isotherm, the results were shown in Fig. 2 and Table S2. The specific surface area and total pore volume of WN are only 1.55 m^2/g and 0.0031 cm^3/g. With the addition of different dyes, the specific surface area and total pore volume of WNs have different increases. If WN is regarded as a network of fibers and different dyes are regarded as tiny particulate matter, the addition of dyes is likely to form a situation similar to particle accumulation on the surface of WNs after doping modification process, thereby increasing the specific surface area and total pore volume. In addition, the specific surface area and total pore volume of WNs modified with the same dye will increase with the increase of the dye concentration. For example, WN-CR-0.01 (4.19 m^2/g and 0.0060 cm^3/g) is greater than WN-CR-0.005 (3.50 m^2/g and 0.0052 cm^3/g), and WN-CR-0.001 (2.86 m^2/g and 0.0046 cm^3/g), WN-CV-0.01 (2.71 m^2/g and 0.0051 cm^3/g) is greater than WN-CV-0.005 (2.50 m^2/g and 0.0042 cm^3/g), and WN-CV-0.001 (2.34 m^2/g and 0.0033 cm^3/g), similarly, WN-MO-0.01 (2.90 m^2/g and 0.0051 cm^3/g) is greater than WN-MO-0.005 (2.80 m^2/g and 0.0049 cm^3/g), and WN-MO-0.001 (2.73 m^2/g and 0.0045 cm^3/g), which can be explained by the above speculation. With the completion of carbonization process, the specific surface area and total pore volume of CWNs are significantly different. Compared with CWN, the specific surface area and total pore volume of carbonized samples mixed with different nitrogen dyes decreased, and the decrease was more obvious with the increase of incorporation concentration. The melting points of CV, MO, and CR are 175, 300, and 360 ℃, respectively, it can be speculated that the high temperature of the carbonization process causes the dye to melt and cover the surface of CWNs. In addition, the added nitrogenous substances generate thermal cracking during the high temperature carbonization

process, and the newly generated substances block part of the pore structure (this can be concluded by comparing Figs. 2d and 2b), thereby reducing the specific surface area of CWNs. It is worth noting that WN-CRs (WN-CR-0.01, WN-CR-0.005, and WN-CR-0.001) and WN-MOs (WN-MO-0.01, WN-MO-0.005, and WN-MO-0.001), whose specific surface area increased most significantly relative to WN in the original sample, declined most significantly after carbonization, which also supported this hypothesis. The activation process is completed with sodium hydroxide as the activator. Under the high temperature condition of no oxygen, the activator will react with the carbon precursor to form carbonate substances through intercalation and embedding, thus forming a new pore structure after cleaning. All BWNs samples, including BWN, showed typical type I isotherms, indicating that BWNs contained a large number of microporous structures (Yang et al., 2023), which was also consistent with the results of the pore size distribution analysis (Fig. 2f). In addition, the results of pore size distribution show that there are some pore structures in BWNs with pore sizes larger than 2 nm, which indicates that BWNs is the microporous materials with partial mesoporous. Both the specific surface area and total pore volume of biochars modified by dye increased first and then decreased, but the maximum specific surface area and total pore volume were found at concentration of 0.005 mol/L (the specific surface area of BWN-CR-0.005, BWN-CV-0.005, and BWN-MO-0.005 are 2533.82, 2750.41, and 2301.40 m^2/g; the total pore volume of BWN-CR-0.005, BWN-CV-0.005, and BWN-MO-0.005 are 1.3186, 1.4027, and 1.2501 cm^3/g). This can be explained by the fact that the nitrogen doped dye molecules are compounded on the surface of the

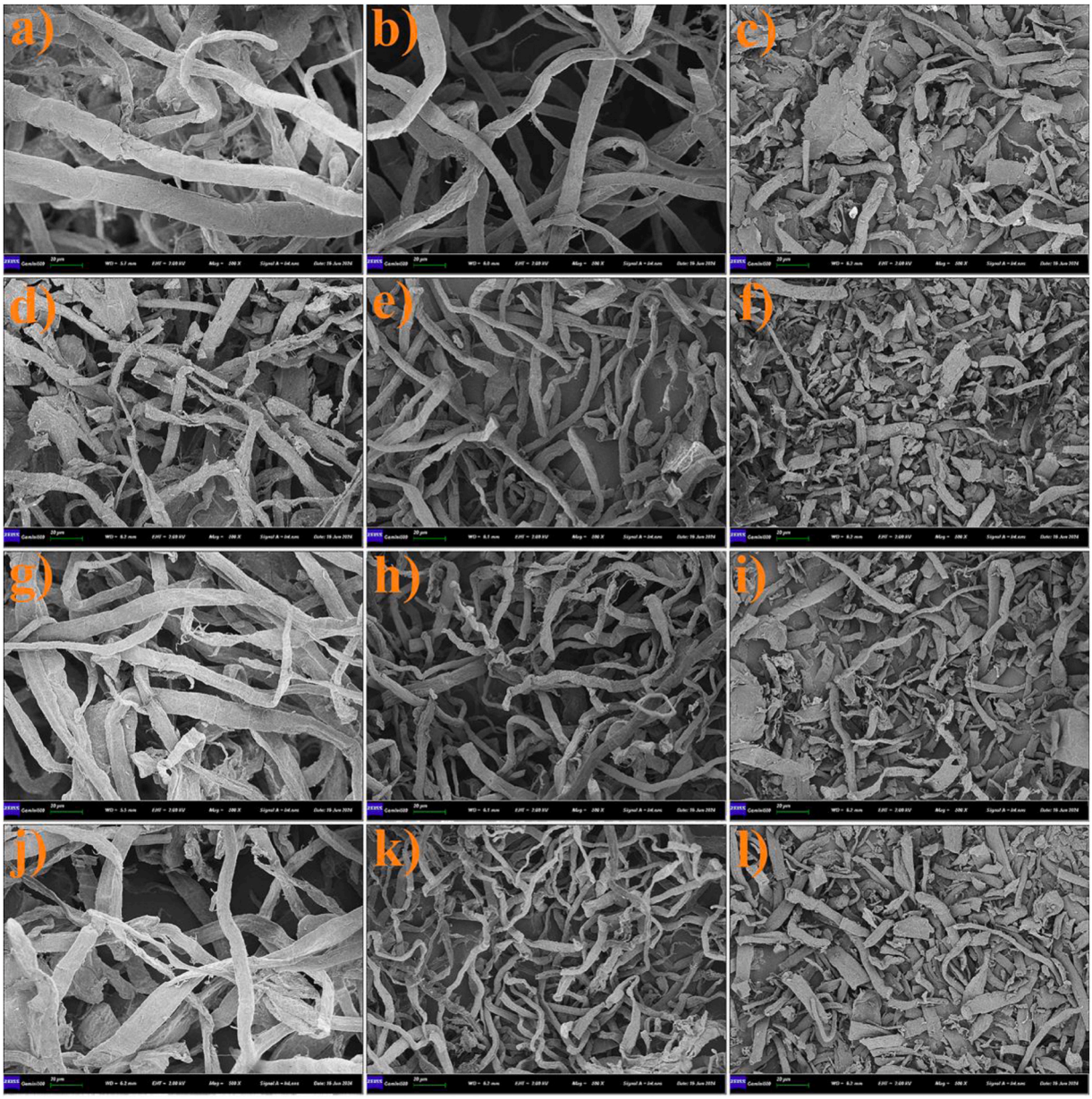

Fig. 3. SEM images of WN, CWN, BWN, WN-CR, CWN-CR, BWN-CR, WN-MO, CWN-MO, BWN-MO, WN-CV, CWN-CV, and BWN-CV.

carbonized sample, and contact with the activator in the molten state during the activation process to complete the activation process, thus generating more pore structure and thereby increasing the specific surface area. However, the addition of too much dye leads to the consumption of more activators in the same activation process, which reduces the activation degree of the whole carbonized sample, thus reducing the activation efficiency. In any case, the addition of appropriate amount of dye was effective in improving the specific surface area and pore structure of biochar. Compared with BWN, the specific surface area of BWN-CR-0.005, BWN-CV-0.005, and BWN-MO-0.005 were increased by 16.6 %, 26.6 %, and 5.9 %, respectively. The total pore volume of BWN-CR-0.005, BWN-CV-0.005, and BWN-MO-0.005 were increased by 7.1 %, 14.0 %, and 1.6 %, respectively, compared with that of BWN. Combined with the results of EDS analysis, BWN-CR-0.005, BWN-CV-0.005, and BWN-Mo-0.005 were selected as BWN-CR, BWN-CV, and BWN-MO models for subsequent studies because of their higher N content, larger specific surface area, and higher total pore volume.

In order to observe the micro-morphology changes of samples, SEM was used to test all samples including WNs,CWNs and BWNs, and the results were shown in Fig. 3. It can be seen that the original samples without carbonization and activation treatment (WN, WN-CR, WN-MO, and WN-CV) all show relatively uniform texture of fibers, most of which are about 10–20 μm in diameter, and different fibers criss-cross to form a three-dimensional spatial network structure. We did not see any significant changes in the incorporation of

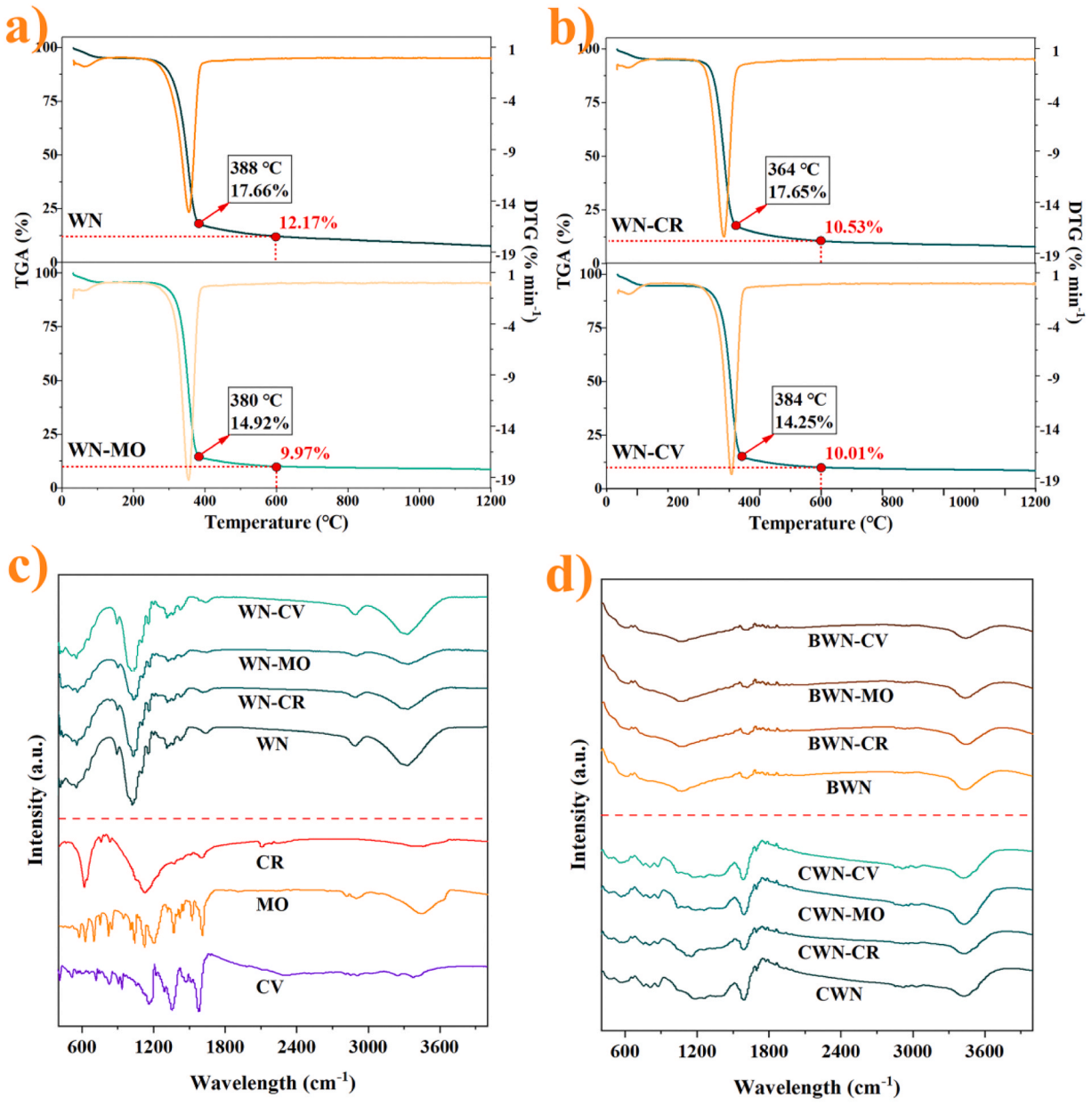

Fig. 4. TGA and DTG curves of (a) WN, WN-MO, (b) WN-CR, and WN-CV. FT-IR of (c) WNs, dyes, (d) CWNs, and BWNs.

high nitrogen dyes, and we speculated that the dye molecules were smaller in size, and it was less easy to distinguish when they were combined with the fibers through adsorption and chemical reactions. However, they are successfully doped onto the fibers, which is not in doubt, as can be seen in the EDS test results (Fig. S1). After carbonization, the fibers of CWNs (CWN, CWN-CR, CWN-MO, and CWN-CV) become wrinkled and thinner in diameter, which is caused by dehydration and thermal cracking of the sample during the carbonization process, and the diameter of the fibers is significantly thinner than that of the corresponding original samples. Similar to most alkali-activated biochar preparation, the activation process caused a large number of fiber breakage and fragmentation in BWNs (BWN, BWN-CR, BWN-MO, and BWN-CV), which could be used to explain why the specific surface area of activated biochars were significantly increased compared with the carbonized samples. It is worth noting that the fragmentation of biochar modified by nitrogen is more obvious, which indicates that the doped dye is likely to play a role in the activation process, which makes the activation process become intense. We will continue to explore this unknown and interesting topic in future studies.

In order to explore the effect of the incorporation of nitrogen-containing dyes on the change of thermal stability of the material, TGA and DTG were used to test the mass changes of WN, WN-CR, WN-CV, and WN-MO with the change of temperature, and the results are shown in Fig. 4a-b. The pyrolysis process can be divided into five stages. The first stage is from room temperature to 100 ℃. At this time, as the temperature rises, the sample begins to become dry. The weight loss in this stage is mainly caused by the escape of water

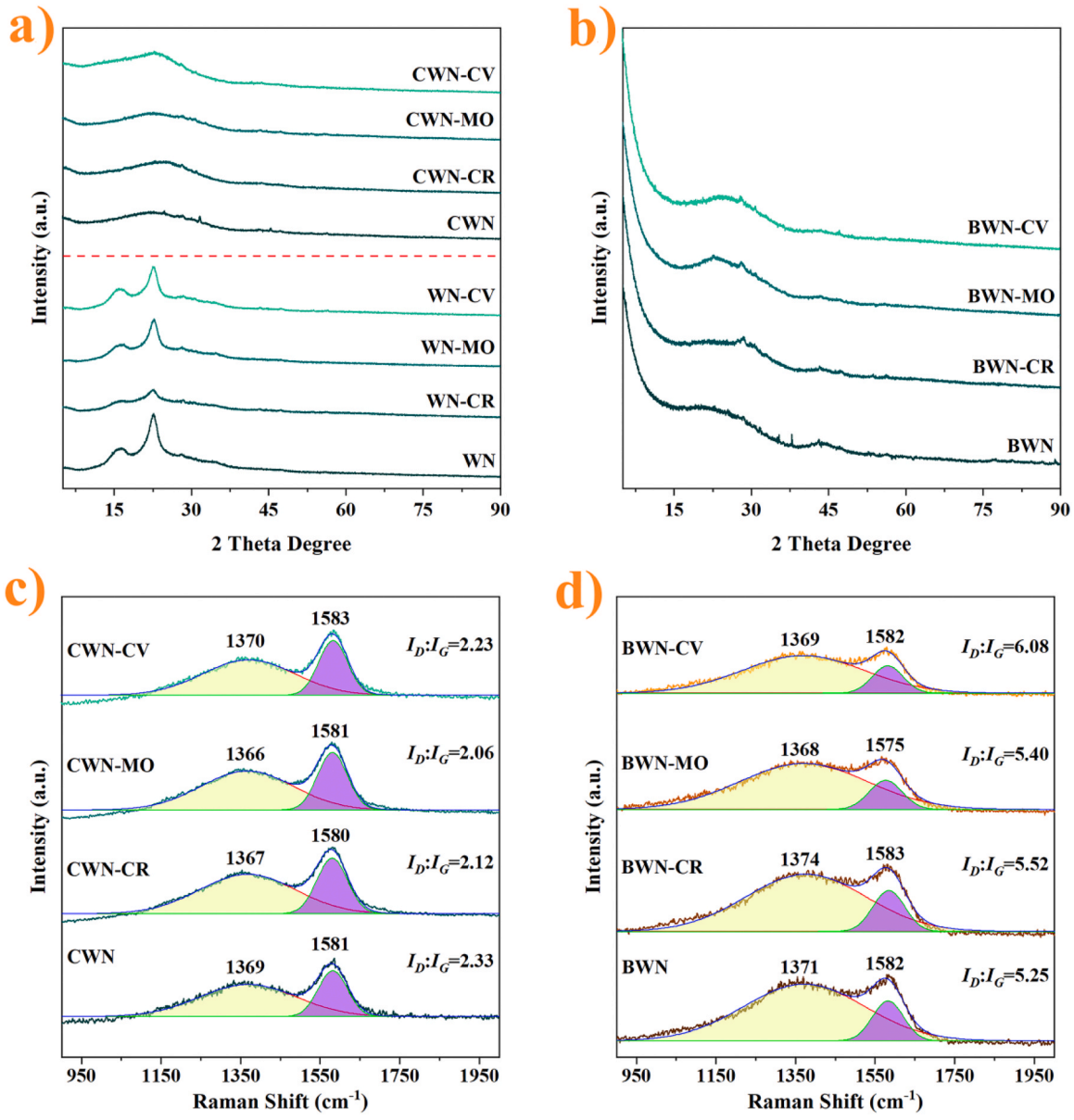

Fig. 5. XRD of (a) WNs, CWNs, and (b) BWNs. Raman spectra of (c) CWNs and (d) BWNs.

adsorbed on the sample surface. The second stage is from 100 ℃ to 300 ℃, and the weight loss in this stage can be classified as higher temperature makes the water bound inside the sample volatilize and part of the lignocellulose thermal cracking. The third stage is from 300 ℃ to TGA "inflection point temperature" (388 ℃ of WN, 380 ℃ of WN-MO, 364 ℃ of WN-CR, and 384 ℃ of WN-CV), and this stage is the most obvious stage of weightlessness, mainly due to the rapid thermal cracking of the sample, which produces a large amount of pyrolysis gas and part of carbon dioxide (Wang et al., 2024). The fourth stage is the process to 600 ℃, the weight of the sample continues to reduce slightly, which may be due to the higher temperature enhances the degree of aromatization of the sample, and the oxygen-containing groups inside the sample are further cracked (Fan et al., 2024). When the temperature exceeds 600 ℃, it comes to the fifth stage, in which the sample has basically completed the carbonization process, the mass is no longer significantly reduced, the physical and chemical properties become stable, and finally the carbon-rich black substance is generated. It is worth noting that the most rapid pyrolysis temperature of WN is slightly higher than the "inflection point temperature" of the other three samples, which can be explained by analogy with the theory of "mixture melting point is lower than pure matter" in the chemical field. After the doping modification of nitrogen-containing dyes, the original WN was relatively pure and regular structure compared with the nitrogen-doped WNs, that is, the nitrogen modification of dyes was not simply mixed with WN, but really incorporated into WN fibers from the microscopic molecular level to achieve "in-situ doping modification". In addition, another major reason for comparison is that the melting point of the incorporated dye molecules is lower than 388 ℃ of WN. When the temperature does not reach this temperature, some of the bonded dyes in the doped sample have begun to undergo thermal cracking process.

The functional groups on the surface of the samples were observed using FT-IR spectroscopy, employing a series of dyes, WNs, CWNs, and BWNs, and the results were shown in Fig. 4c-d. It can be seen that in addition to peaks at 3378–3452 cm^{-1} representing N-H bonds in the dye samples, there are many peaks distributed between 500 and 1700 cm^{-1}, representing C-H, C═O, C-C, and aromatic rings, which are typical characteristic peaks of dye molecules. At the same time, multiple peaks at 1000–1700 cm^{-1} in WN are the characteristic peaks of lignocellulose structure. After modification, most peaks in this region still exist in WNs, and they cannot be further analyzed because they overlap with the characteristic peaks of dyes in many places. However, it is worth noting that, the peaks representing -OH at 3328 cm^{-1} in WN originally produced a slight displacement polarization (3332 cm^{-1} for WN-CR, 3332 cm^{-1} for WN-MO, and 3331 cm^{-1} for WN-CV) after the incorporation of dye molecules, which indicated that during the doping process, the dye produced a strong hydrogen bond with WN, which also represented the successful incorporation of the dyes. After the carbonization process, several typical peaks appear more obvious, namely the peaks at 1015–1024 cm^{-1} representing C-N and C-O, the peaks at 1156–1184 cm^{-1} representing carbonyl groups of a conjugated structure, the peaks at 1588–1593 cm^{-1} representing aromatic rings, and the peaks at 3424–3429 cm^{-1} representing N-H and -OH. Similarly, there are several very significant peaks in the activated biochar, in addition to the more powerful peaks representing C-N and C-O at 1056–1076 cm^{-1} and N-H and -OH at 3432–3438 cm^{-1}, there are also have the peaks representing C═O stretching of the aromatic rings at 1618–1619 cm^{-1} (Shi et al., 2024; Zhang et al., 2025; Cui et al., 2024). The above results not only prove the successful incorporation of dyes in the modification process, but also indicate that the surface of the prepared biochars contains a large number of functional groups and unsaturated keys, which are likely to provide active sites for the use of biochars as adsorbents.

In order to observe the change of crystallinity of the samples, XRD tests were conducted on WNs, CWNs, and BWNs, and the results were shown in Fig. 5a-b. In the original sample (WNs), the samples all had two peaks at 17 and 22 °, representing cellulose crystalline structures from lignocellulose (Padilla et al., 2024). It is worth mentioning that the two peaks in WN-CR, WN-CV, and WN-MO are weakened compared with WN, which indicated that the crystallinity of the samples changes with the addition of dye. After the high temperature carbonization process, the crystallization peak representing cellulose disappeared and was replaced by a wide peak at about 23.5 °, which can be explained by the emergence of a large number of carbon-containing aromatic structures after the samples pyrolysis at high temperatures. Finally, after the activation process of activator etching, in addition to the wide peak (002) at 23.5 °, a wide peak with weak signal appeared at 43 °, also representing the graphite crystalline structure (100) (Mele et al., 2024) indicating that biochar BWN, BWN-CR, BWN-MO, and BWN-CV are all amorphous carbon materials with local ordered structure.

In order to observe the change of carbon defects of the samples, Raman tests are performed on WNs, CWNs, and BWNs, and the results are shown in Fig. 5c-d. Both CWNs and BWNs contain two marker peaks at 1366–1374 and 1575–1583 cm^{-1}, namely, D peak representing amorphous carbon structure and G peak representing graphite structure. The two carbon defect structures represent different hybridization modes of carbon atoms, with peak D representing sp3 hybridization and peak G representing sp2 hybridization. Carbon atoms with different hybridization modes mean atomic loss or lattice distortion, thus affecting the electronic structure and chemical properties of carbon materials (Mao et al., 2024; Li et al., 2023). The intensity ratio of D-peak to G-peak (I_D/I_G) is often used to detect changes in carbon defects in carbon materials, and is also an important parameter to monitor changes in the structure of carbon atoms in carbon materials. The I_D/I_G values of CWN, CWN-CR, CWN-MO, and CWN-CV were 2.33, 2.12, 2.06, and 2.23, which meant that CWNs samples contain a large number of amorphous structures. After activation, the I_D/I_G values of BWNs increased further (5.25, 5.52, 5.40, and 6.08 for BWN, BWN-CR, BWN-MO, and BWN-CV), indicating the formation of more amorphous structures, which may be caused by the violent reaction caused by the etching of the activator in the activation process. A large number of amorphous structures may result in a larger specific surface area and more abundant pore structure in biochar samples, which is also consistent with the results of N_2 adsorption-desorption isotherm tests.

In order to study the charge on the surface of biochars, Zeta potential tests were performed on WNs, CWNs, and BWNs, and the results were shown in Fig. S2. When the solution is at a specific pH and the net charge on the solid surface is zero, the pH of the solution at this time is the pH_{pzc} of the sample (Singh et al., 2016). The pH_{pzc} of BWN, BWN-CV, BWN-MO, and BWN-CR were 4.60, 4.66, 5.32, and 5.77. As pH increased, all biochar surfaces became more negatively charged, suggesting that BWNs, including BWN, were better suited to deal with positively charged contaminants at high pH. In addition, it can also be easily found that after nitrogen doping modification, the absolute values of pH_{pzc} of biochars are slightly higher than that of BWN, indicating that the surface charge density of

nitrogen-doped biochars are higher, which may be because the incorporation of nitrogen atoms leads to the introduction of more electrons on the surface of biochars.

The surface chemical bond price and electronic state of biochar are one of the important parameters to determine its performance, thus, XPS test was performed on the samples and their C1s, O1s, and N1s compositions were fitted and analyzed, and the results were shown in Fig. 6. The surfaces of BWNs (including BWN) are all composed of C, O, and N elements, and the N content of BWN-CR (3.51 %), BWN-CV (2.53 %), and BWN-MO (1.74 %) is higher than that of BWN (1.16 %) after incorporation of dyes, which indicated that N-containing dyes have successfully modified biochars. The C1s high-resolution spectra of the four biochars (BWN, BWN-CR, BWN-CV, and BWN-MO) were basically not very different, and both they all had three distinct peaks at 287.35–287.88, 284.47–284.95, and 283.91–283.99 eV, corresponding to the C═O, C-O, and C-C bonds (Li et al., 2024) There are some differences in the results of O1s high-resolution spectra. BWN contains three fitting peaks, namely, Quinones at 530.65 eV, C═O at 531.64 eV, and -OH at 533.18 eV. BWN-MO contains three fitting peaks, namely, C═O at 531.52 eV, -OH at 533.12 eV, and O═C-O at 535.05 eV. Both BWN-CV and BWN-CR contain four fitting peaks, except for Quinones at 530.35–530.66 eV, C═O at 531.35–531.63 eV, and -OH at 533.19–533.33 eV, they also contains C-O at 532.35 eV and O═C-O at 535.10 eV (Guo et al., 2024), respectively, which fully proves

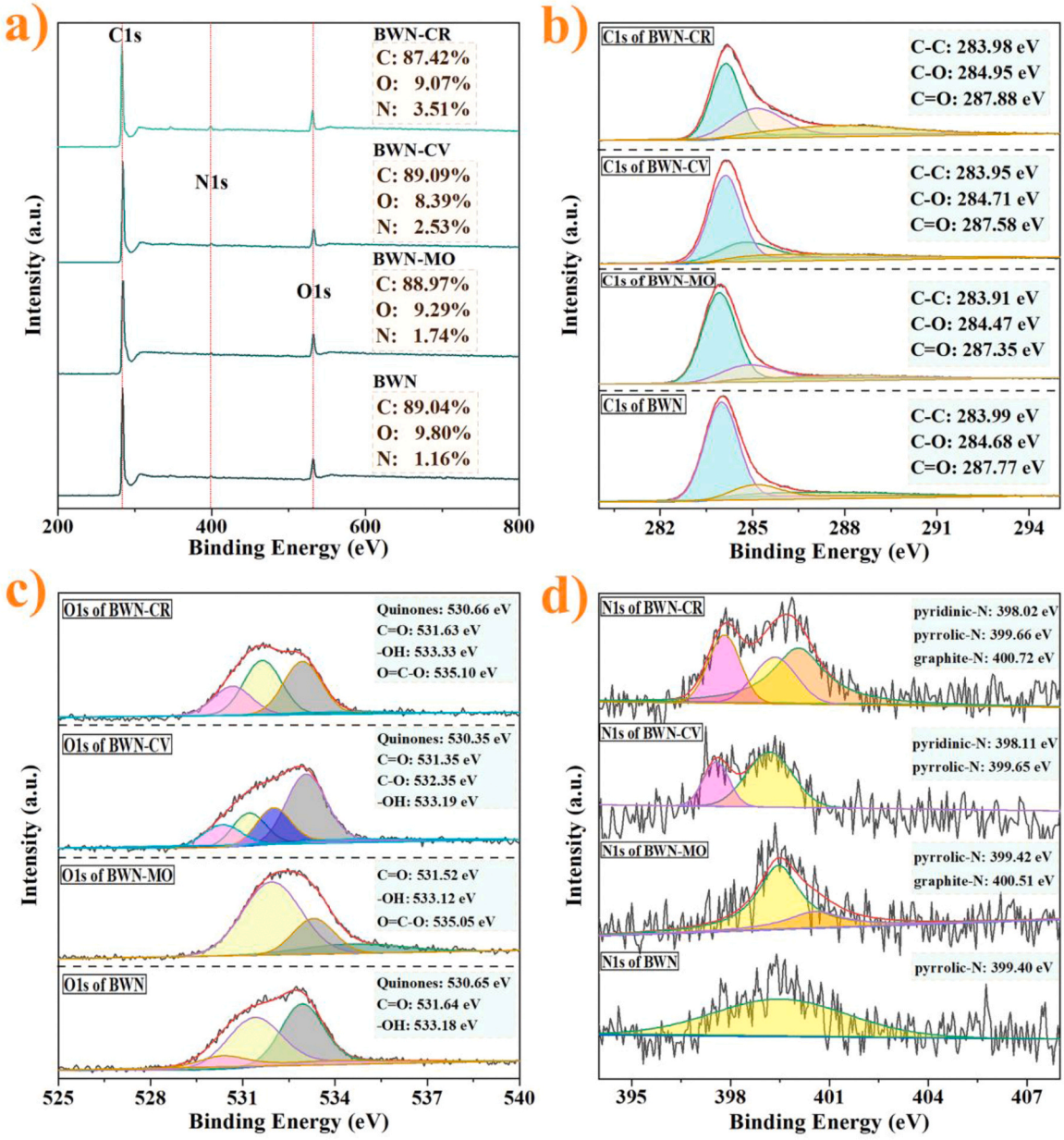

Fig. 6. (a) XPS, (b) C1s, (c) O1s, and (d) N1s of BWNs.

that different dyes bind WN in different ways. The N1s high-resolution spectrum of biochars had the largest difference, and it can be clearly seen that the incorporation and modification of dyes successfully enriched the types of N elements in biochars. BWN only contains pyrrolic-N at 399.40 eV, and these nitrogen elements may come from the nitrogen-containing substances (proteins or amino acids, etc.) remaining in lignocellulosic biomass in raw material WN. Both BWN-MO and BWN-CV contain two types of N, in addition to pyrrolic-N at 399.42–399.65 eV, graphite-N at 400.51 eV and pyridinic-N at 398.11 eV, respectively. BWN-CR contains three types of N, pyridinic-N at 398.02 eV, pyrrolic-N at 399.66 eV, and graphite-N at 400.72 eV (Lyu et al., 2024). In general, pyridinic-N is nitrogen connected between two carbon atoms on the edge of the biochar graphite structure, and it is easily oxidized because of the presence of lone pairs of electrons. Pyrrolic-N contains two *p* electrons conjugated with the π bond, so it is likely to provide π-π interaction for the adsorption process. Graphite-N refers to nitrogen attached to three carbon atoms in the graphite base and is relatively stable. After the modification of nitrogen-containing dyes, compared with BWN, biochars contains newly generated N type, which is likely to provide different promotion effects in the process of adsorption of pollutants. The emergence of graphite-N type indicates that this nitrogen doping method is not only a simple mixing of nitrogen elements, but also may complete a more solid and stable modification similar to "in-situ doping" from the molecular level of biochar.

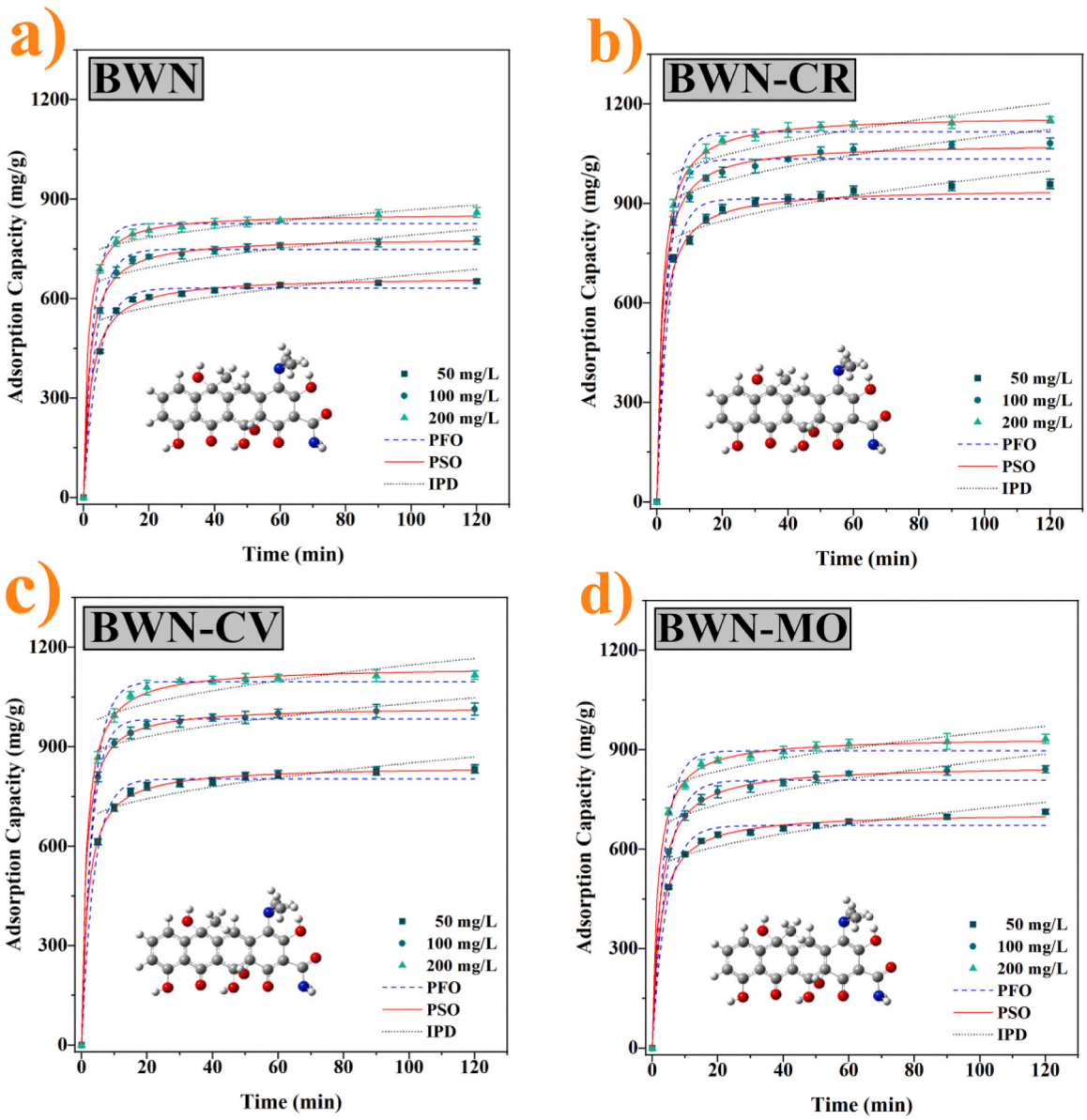

Fig. 7. Adsorption kinetics of (a) BWN, (b) BWN-CR, (c) BWN-CV, and (d) BWN-MO at 303 K.

3.3. Adsorption experiment results

Adsorption kinetics was employed to investigate the trend of four materials in reaching adsorption equilibrium at different concentrations of TH solution (50, 100, 200 mg/g). The obtained results were then fitted with three kinetic models (namely PFO, PSO, and IPD) with the fitted results and parameters displayed in Fig. 7a-d and Table S3. The four biochars adsorbed TH rapidly in the first 20 min, then the adsorption process started to slow down and finally reached the adsorption equilibrium at 120 min. From the results obtained, it can be seen that the adsorption capacity of BWN (861.33 mg/g) after nitrogen doping of dyes is enhanced to different degrees, and the higher enhancement is found in BWN-CR (1159.05 mg/g) and BWN-CV (1120.04 mg/g), which may be caused by the different amounts of different kinds of dye molecules retained on the BWN. By fitting the obtained adsorption data to the PFO and PSO kinetic models, the fitted results showed that the correlation coefficients R^2 of the PSO for the four materials (BWN: 0.9969–0.9994, BWN-CR: 0.9964–0.9997,BWN-CV: 0.9990–0.9998, BWN-MO: 0.9992–0.9996) were higher than the R^2 of PFO (BWN: 0.9835–0.9849, BWN-CR: 0.9816–0.9882, BWN-CV: 0.9608–0.9859, BWN-MO: 0.9875–0.9889) and the theoretical adsorption amount of PSO was closer to the adsorption amount measured in the actual experiments, which indicated that PFO kinetic model is not suitable for describing the adsorption process of the four materials, and the PSO kinetic model can better match the adsorption process of the four

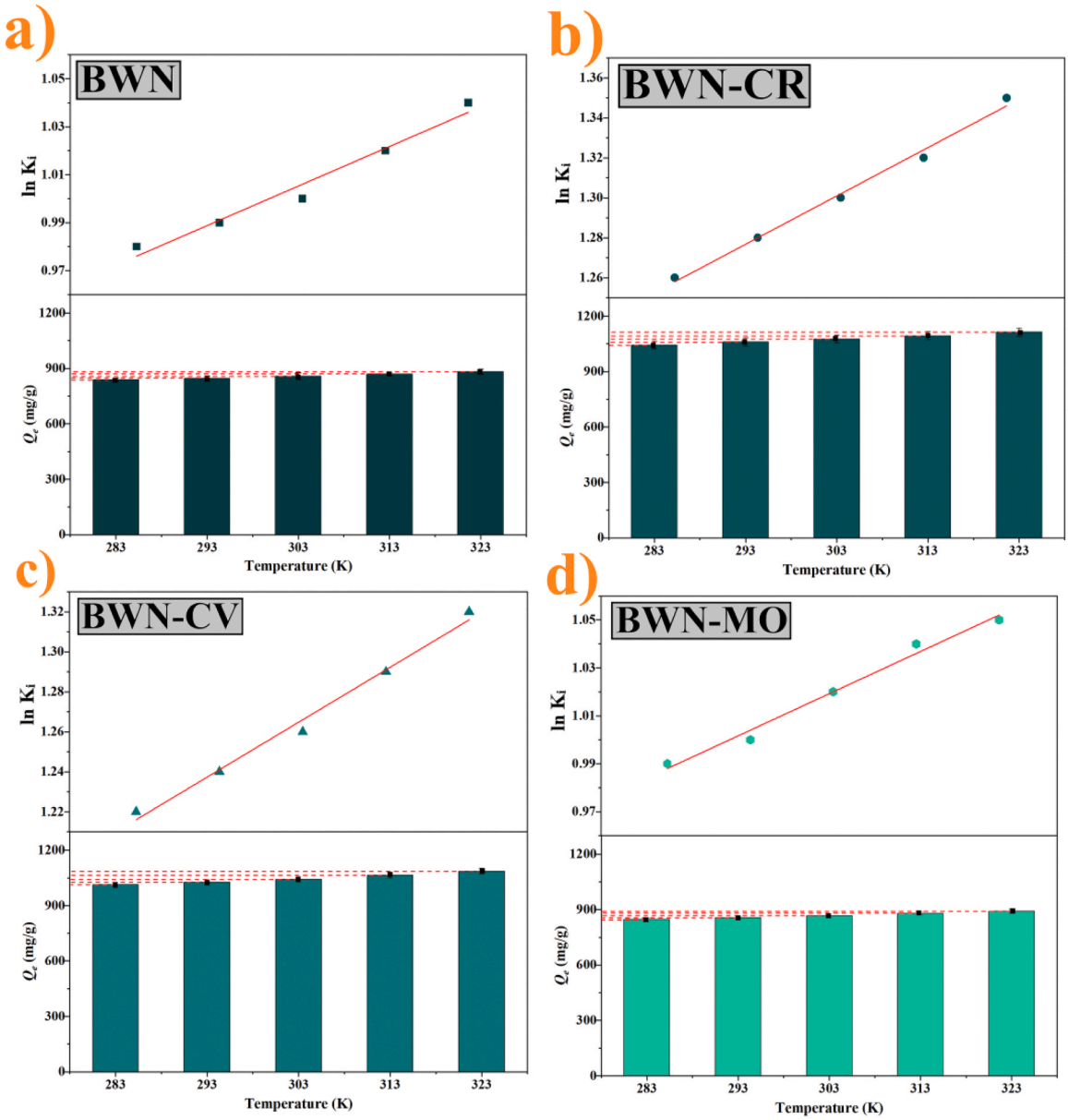

Fig. 8. Effect of temperature on the adsorption capacity of (a) BWN, (b) BWN-CR, (c) BWN-CV, and (d) BWN-MO.

materials, so that it can be inferred that the adsorption process is dominated by chemisorption (Minaei et al., 2024). For the IPD model, the fitted R^2 values were significantly smaller than those of PSO and PFO, with correlation coefficients of 0.6120–0.7356, 0.6874–0.7941, 0.5659–0.6744, and 0.7160–0.7480 for the four materials, respectively. which showed that the adsorption process is not controlled by the IPD model.

The adsorption isotherm curve represents the relationship between the concentration of solute molecules present in the two distinct phases at equilibrium, which is reached at a particular temperature at the interface between the two phases. The adsorption process of biochars is reflected in this equilibrium curve, indicating the initial concentration of adsorbates. In order to fit the obtained data, the Langmuir and Freundlich isotherm models were utilised. According to the Langmuir model, adsorption occurs in a homogeneous manner in terms of energy across different adsorption sites and surface coverages. Adsorption occurs with the same energy efficiency across different adsorption sites and different surface coverages. In this instance, the substance forms a single layer, with no intermolecular forces present between the adsorbed molecules. It is presumed that the adsorbed molecules are not in any way interacting with one another. It is postulated that a monolayer of adsorption will form, wherein there will be no intermolecular interaction between the adsorbed molecules. The Freundlich isotherm model is employed to delineate the adsorption of non-uniform and

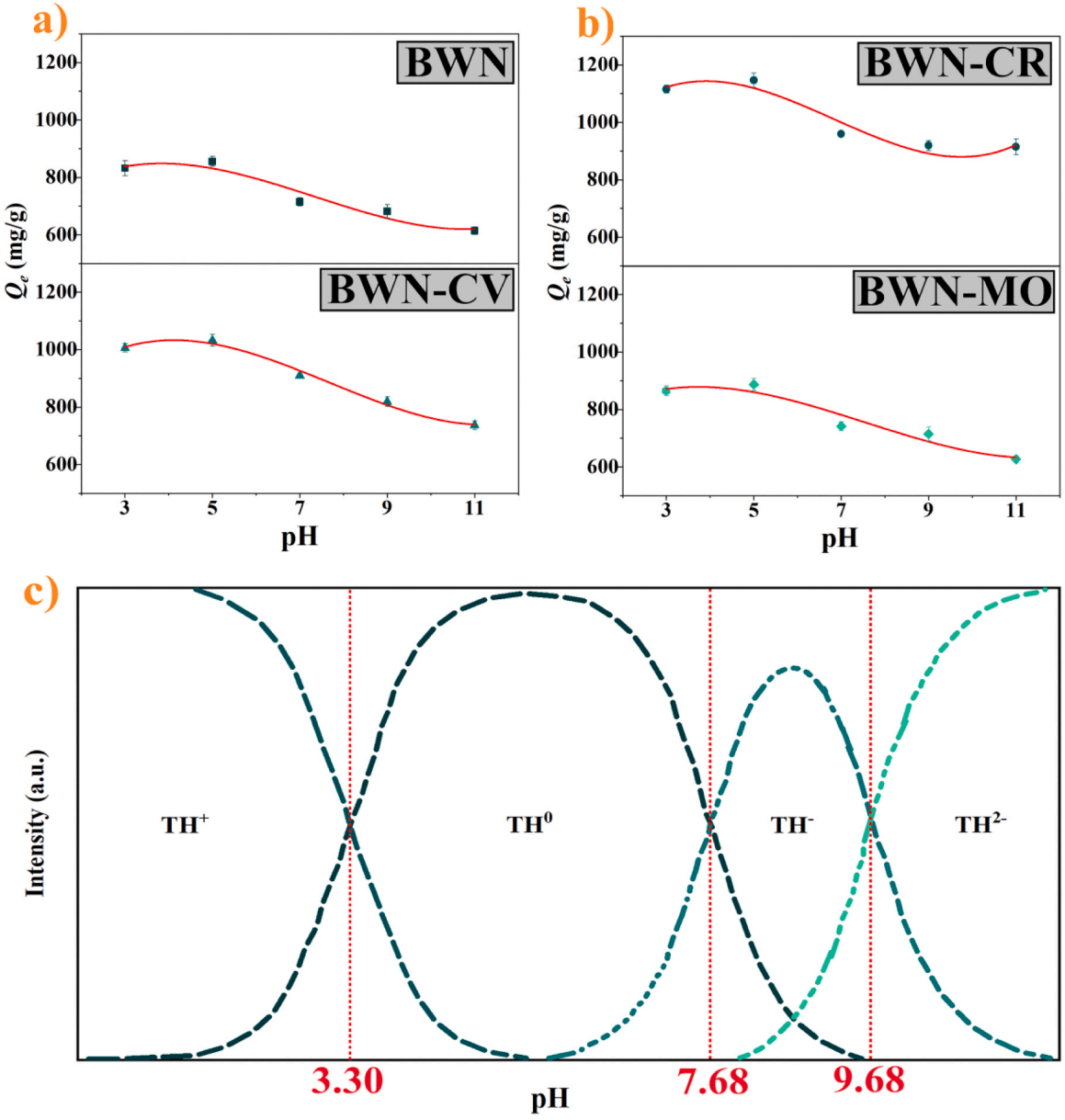

Fig. 9. Effect of pH on the adsorption capacity of (a) BWN, BWN-CV, (b) BWN-CR, and BWN-MO. (c) The distribution of charged forms of TH in different pH values.

heterogeneous phases in heterogeneous systems. It is an isotherm model that is employed in the field of adsorption. The molecules of the adsorbent form a multimolecular layer on the surface of the solid. The obtained data and after fitting the results were shown in Fig. S3 and Table S4, the adsorption of TH by the samples gradually increased with the increase of initial concentration and the magnitude of the increase gradually decreased, which may be due to the limited number of adsorption sites on the surface of the samples, which in turn led to the saturation of adsorption by the samples. The fitted results showed that the adsorption data fitted poorly to the Langmuir isotherm model and better to the Freundilich, with R^2 reaching 0.9961, 0.9931, 0.9911, and 0.9923 for BWN, BWN-CR, BWN-CV, and BWN-MO, respectively, which suggests that the adsorption process may be multilayer adsorption (Koulouri et al., 2024; Cheng et al., 2023).

It is evident that temperature plays a pivotal role in the adsorption process. To gain further insight into the influence of temperature on adsorption, further investigation is required, the researchers used thermodynamic modelling and parametric indices to calculate the effect of temperature on adsorption. The impact of materials on the adsorption of antibiotic TH at varying temperatures (283, 293, 303, 313 and 323 K) was examined, with the findings utilized to calculate thermodynamic parameters. The results are presented in Fig. 8a-d and Table S5. It can be observed that the Q_e of the samples for TH increased with an increase in temperature. The thermodynamic parameter ΔG is employed to represent the Gibbs free energy. The thermodynamic parameter, ΔG, is most commonly utilized as a metric to evaluate the spontaneity and equilibrium of a given reaction process under constant temperature and pressure conditions. A negative value of ΔG signifies the occurrence of the reaction process in a spontaneous manner (Li et al., 2024). The standard enthalpy change, ΔH, represents a thermodynamic parameter that is typically employed in the context of indicating the increase in enthalpy associated with a specific reaction process. A positive value of ΔH indicates that the reaction process is endothermic. In contrast, when ΔH is less than 0, this implies that the reaction process is exothermic (Azri et al., 2024). The symbol S represents entropy, which can be defined as the degree of freedom of a system undergoing a given chemical reaction. In accordance with the second law of thermodynamics, an increase in entropy ($\Delta S>0$) can be described as follows: an increase in the reaction volume serves to enhance the degree of freedom of the reaction system. The degrees of freedom of the action system increase, for example, as a consequence of an increase in the amount of gas or new substance produced in the reaction. In the case that ΔS is less than zero, entropy increases, which may be interpreted as an expansion in the number of degrees of freedom of the reaction system. An illustrative example of this phenomenon is the production of greater quantities of gas or a new substance in a chemical reaction (Lin et al., 2020). The thermodynamic parameters obtained by taking the adsorption data and calculating them showed that ΔG was negative for the four materials, indicating that the adsorption process was spontaneous. The values of ΔH were 1.20, 1.86, 2.00, and 1.38 kJ mol^{-1}, indicating that the adsorption process was heat absorbing and that the reaction process could be facilitated with an increase in temperature. The values of ΔS were all positive when the sample adsorbed TH, indicating that the interfacial freedom between the sample and the TH molecules increased with increasing temperature.

The pH of the solution is also one of the factors affecting the adsorption process, the adsorbent will show different adsorption characteristics at different pH of the solution, this is due to the fact that the pH will change the form of ions present in the solution and will also lead to a change in the properties of the adsorbent. The adsorbent surface is positively charged when the solution pH is less than pH_{pzc}. Also, as shown in Fig. 9c, TH has different ionic presence forms at different pH (pH<3.30 for TH^+, 3.30 <pH<7.68 for TH^0, 7.68 <pH<9.68 for TH^-, pH>9.68 for TH^{2-}) (Chen et al., 2021; Jin et al., 2024). The results of the adsorption of TH by the four adsorbents at different pH are shown in Fig. 9a-b, at pH= 5 the adsorption of all the four adsorbents is at its maximum and it decreases with the increase of pH, when pH= 3, the solution is mainly in the form of TH^+ and the materials are positively charged on the surface and hence electrostatic repulsion occurs, similarly, when pH is 7, all the four materials surfaces are negatively charged and although

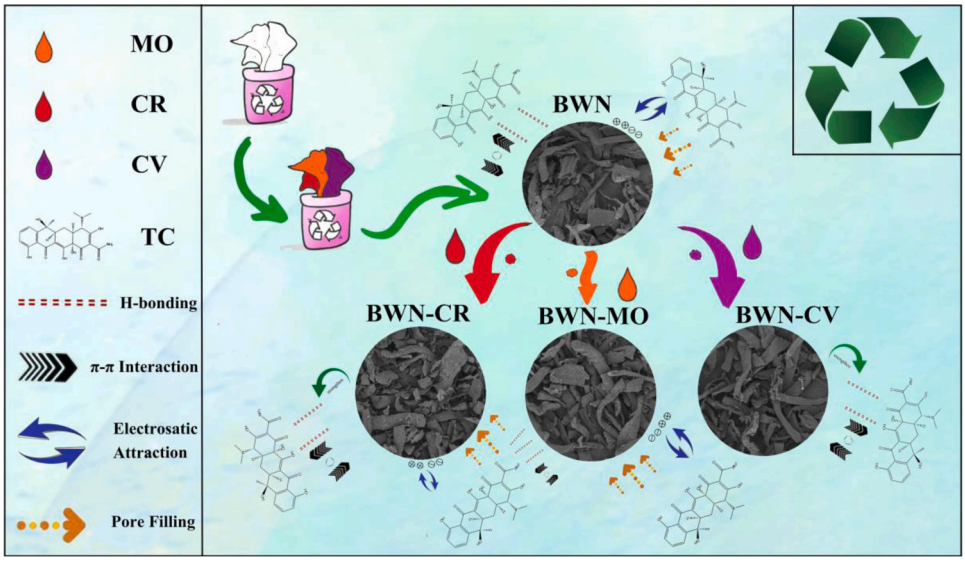

Fig. 10. The possible adsorption mechanism of biochars.

present in the solution in the form of TH^0, they are also being transferred to TH^- (pH=7.68) and hence may lead to a gradual decrease in the adsorption of the materials onto the adsorbent after pH= 7 due to electrostatic repulsion.

The cyclic regeneration capacity of the adsorbent is an important factor in examining the cyclic effect of the adsorbent. Here, we utilized thermal regeneration to recycle the material, simply by recovering the adsorbed biochar, drying it, and subsequently placing it into a tube furnace for thermal regeneration under nitrogen protection at 500 °C for 60 min. The thermally regenerated biochar was put into the new solution again. The results are shown in Fig. S4. After 10 cycles, the removal rate of TH by the four samples could still be maintained at more than 65 %, indicating that the samples have good stability and regeneration ability, and can be used to remove pollutants from water. In parallel, we conducted a comparative analysis of the adsorption capacity of biochar with other adsorbents (Table S6). The results of our investigation indicate that the adsorption capacity of biochar is significantly higher than that of other adsorbents. This further substantiates the considerable potential of biochar in the control of water pollution. Concurrently, the local lake water was sampled and subjected to the addition of varying concentrations of antibiotics, thereby simulating the removal process in the actual environment. The findings(Fig. S5) indicated that the samples exhibited 100 % removal in wastewater with TH concentrations spanning a range of 10–50 mg g^{-1}.

After the above analyses, it was shown that the adsorption mechanism may involve pore filling, hydrogen bonding, π-π interaction and electrostatic attraction. The nitrogen adsorption and desorption isotherm data showed that the specific surface area of BWN (2173.13 m^2 g^{-1}) was increased to different degrees after nitrogen doping with different dyes (BWN-CR: 2533.82 m^2 g^{-1}; BWN-CV: 2750.41 m^2 g^{-1}; and BWN-MO: 2301.40 m^2 g^{-1}), and the larger specific surface area can provide more adsorption sites and material transfer capacity for the material. And as shown in Table S7, the specific surface area of the adsorbed materials had a significant decrease to 271, 434, 396 and 385 m^2 g^{-1}, respectively. The larger specific surface area can provide more adsorption sites and substance transfer capacity for the materials, which is one of the important reasons for the higher adsorption capacity of the nitrogen-doped materials. The XPS and EDS results showed that the activated samples of BWN after nitrogen doping increased part of the pyrrolic-N and pyridinic-N, which increased the hydrogen bonding to a certain degree, and it can be speculated that there may be π-π interactions between the TH molecules and the unsaturated functional groups of the activated samples by FT-IR. And at pH= 3, 7, 9, and 11, the adsorption of TH by the samples had different degrees of electrostatic repulsion, while the highest adsorption was observed at pH= 5, when TH was present in solution in the form of TH^0, indicating that electrostatic attraction played a relatively small role in the adsorption process.

4. Conclusion

In this work, domestic refuse WN was used as raw material, modified by different dyes impregnation, and N-doped modified biochars were prepared by carbonation and activation. The results showed that the addition of dyes not only optimized the physical and chemical properties of biochars, but also greatly improved the adsorption performances. The specific surface areas of BWN-CR, BWN-CV, and BWN-MO were up to 2533.82, 2750.41, and 2301.40 m^2/g, respectively, which increased by 16.6 %, 26.6 %, and 5.9 % compared with that of BWN (2173.13 m^2/g). In addition, the content of nitrogen atoms in the modified biochars increased by 0.50–2.03 times compared with that in the undoped biochar (BWN). After kinetics and isotherm experimental data fitting indicated that the adsorption process may be chemisorption and multilayer adsorption. The possible adsorption mechanisms are pore filling, hydrogen bonding, π-π interaction and electrostatic attraction. Among them, pore filling dominates the adsorption process. Finally, in the adsorption experiment using TH model, the adsorption capacities of all N-doped biochars (BWN-CR, BWN-CV, and BWN-MO) were greater than that of most adsorbents including BWN. After 10 cycles of use, the biochars can still maintain more than 65 % of the performance, indicating their stable regeneration ability. This work not only prepared a series of biochars that can be used to efficiently remove antibiotics from water, but more importantly, the different effects of different high-nitrogen dyes on doping modification were compared and analyzed, and the possible mechanisms involved in the experiment were discussed, which provided a new strategy for high-value utilization of WN in domestic waste and further release the application potential of secondary resources.

CRediT authorship contribution statement

Guang Chen: Supervision, Resources. **Chunjie Tian:** Resources. **Siji Chen:** Writing – original draft, Software, Resources, Methodology, Investigation, Funding acquisition, Formal analysis, Data curation. **Zhongwen Zhou:** Methodology, Formal analysis. **Yiping Jin:** Writing – original draft, Software, Methodology, Formal analysis, Data curation.

Declaration of Competing Interest

The authors declare that they have no known competing financial interests or personal relationships that could have appeared to influence the work reported in this paper.

Acknowledgement

Thanks for the supported by Jilin Province Science and Technology Development Plan Project (20240303086NC).

Appendix A. Supporting information

Supplementary data associated with this article can be found in the online version at doi:10.1016/j.eti.2024.103921.

Data Availability

The authors are unable or have chosen not to specify which data has been used.

References

Azri, N., Chebbi, R., Ouakouak, A., Hecini, L., Isinkaralar, K., Fadel, A., Bokov, D.O., Prakash, C., Hosseini-Bandegharaei, A., 2024. Single and binary adsorption of paracetamol and diclofenac onto biochar produced from pepper stem: which adsorption properties change in the binary system. Colloid Surf. A. 694, 134136. https://doi.org/10.1016/j.colsurfa.2024.134136.

Basta, A.H., Lotfy, V.F., 2023. Sustainable development of pulping by-product for limiting its pollution risk and production new aerogel-based carbon nanostructures for dyes adsorption. J. Clean. Prod. 428, 139275. https://doi.org/10.1016/j.jclepro.2023.139275.

Chen, Y., Liu, J., Zeng, Q., Liang, Z., Ye, X., Lv, Y., Liu, M., 2021. Preparation of Eucommia ulmoides lignin-based high-performance biochar containing sulfonic group: synergistic pyrolysis mechanism and tetracycline hydrochloride adsorption. Bioresour. Technol. 329, 124856. https://doi.org/10.1016/j.biortech.2021.124856.

Cheng, N., Wang, B., Chen, M., Feng, Q., Zhang, X., Wang, S., Zhao, R., Jiang, T., 2023. Adsorption and photocatalytic degradation of quinolone antibiotics from wastewater using functionalized biochar. Environ. Pollut. 336, 122409. https://doi.org/10.1016/j.envpol.2023.122409.

Cui, J., Wei, L., Ning, C., Zhang, F., Cui, J.Peng X., 2024. Highly-efficient persulfate activation by nitrogen-doped biochar derived from dewatered sewage sludge for 2,4-dichlorophenol removal: Process and mechanism. J. Environ. Chem. Eng. 12, 112561. https://doi.org/10.1016/j.jece.2024.112561.

Fan, Y., Fu, F., Yang, D., Liu, W., Qiu, X., 2024. Thiocyanogen-modulated N, S Co-doped lignin hierarchical porous carbons for high-performance aqueous supercapacitors. J. Colloid Interf. Sci. 667, 147–156. https://doi.org/10.1016/j.jcis.2024.04.099.

Farmanbordar, S., Javid, A., Amiri, H., Denayer, J.F.M., Karimi, K., 2024. Enhanced biobutanol production with sustainable Co-substrates synergy from paper waste and garden waste with municipal biowaste. Biomass Bioenerg. 186, 107262. https://doi.org/10.1016/j.biombioe.2024.107262.

Fu, Z., Zhao, J., Guan, D., Wang, Y., Xie, J., Zhang, H., Sun, Y., Zhu, J., Guo, L., 2024. A comprehensive review on the preparation of biochar from digestate sources and its application in. Environ. Pollut. Remed. Sci. Total Environ. 912, 168822. https://doi.org/10.1016/j.scitotenv.2023.168822.

Guo, W., Wang, Y., Chen, W., Xu, G., Zhu, G., Xie, G., Xu, L., Fang, Z., Zhang, Q., Yang, H., 2024. Insight into the synergistic influence of nitrogen-doped biochar and NH_3 on selective production of 4-vinyl phenol from biomass catalytic pyrolysis by coupling catalyst in-situ regeneration. Ind. Crop. Prod. 214, 118520. https://doi.org/10.1016/j.indcrop.2024.118520.

Jin, Y., Zhang, B., Guo, Z., Lin, J., Chen, G., Chen, S., Su, Y., 2024. Biochar with improved performance prepared based on "micro-explosive reaction" conjecture for effective removal of antibiotics. Fuel 361, 130733. https://doi.org/10.1016/j.fuel.2023.130733.

Khedulkar, A.P., Dang, V.D., Thamilselvan, A., Doong, R., Pandit, B., 2024. Sustainable high-energy supercapacitors: metal oxide-agricultural waste biochar composites paving the way for a greener future. J. Energy Storage 77, 109723. https://doi.org/10.1016/j.est.2023.109723.

Khedulkar, A.P., Pandit, B., Dang, V.D., Doong, R., 2023. Agricultural waste to real worth biochar as a sustainable material for supercapacitor. Sci. Total Environ. 869, 161441. https://doi.org/10.1016/j.scitotenv.2023.161441.

Koulouri, M.E., Templeton, M.R., Fowler, G.D., 2024. Enhancing the nitrogen and phosphorus content of faecal-derived biochar via adsorption and precipitation from human urine. J. Environ. Manag. 352, 119981. https://doi.org/10.1016/j.jenvman.2023.119981.

Li, Y., Awasthi, M.K., Sindhu, R., Binod, P., Zhang, Z., Taherzadeh, M.J., 2023. Biochar preparation and evaluation of its effect in composting mechanism: a review. Bioresour. Technol. 384, 129329. https://doi.org/10.1016/j.biortech.2023.129329.

Li, J., Mei, M., Han, Y., Hong, M., Man, Y., 2020. Life cycle cost assessment of recycled paper manufacture in China. J. Clean. Prod. 252, 119868. https://doi.org/10.1016/j.jclepro.2019.119868.

Li, H., Zhen, F., Zhang, Q., Song, Y., Zhang, L., Qu, B., 2024. Preparation of porous lignocellulose biochar adsorbent by cold isostatic pressing pretreatment and study on Hg (II) adsorption properties of C and N dual activity sites. Int. J. Biol. Macromol. 274, 133479. https://doi.org/10.1016/j.ijbiomac.2024.133479.

Lin, R., Liang, Z., Yang, C., Zhao, Z., Cui, F., 2020. Selective adsorption of organic pigments on inorganically modified mesoporous biochar and its mechanism based on molecular structure. J. Colloid Interf. Sci. 573, 21–30. https://doi.org/10.1016/j.jcis.2020.03.112.

Lyu, H., Wang, X., Li, P., Yan, P., Tang, J., 2024. Mn/Co bimetallic catalyst immobilized on N-doped biochar for enhanced photocatalytic degradation of sulfanilamide in water. Appl. Catal. B-Environ. Energy 354, 124123. https://doi.org/10.1016/j.apcatb.2024.124123.

Man, Y., Han, Y., Li, J., Hong, M., 2019. Review of energy consumption research for papermaking industry based on life cycle analysis. Chin. J. Chem. Eng. 27, 1543–1553. https://doi.org/10.1016/j.cjche.2018.08.017.

Man, Y., Han, Y., Liu, Y., Lin, R., Ren, J., 2020. Multi-criteria decision making for sustainability assessment of boxboard production: a life cycle perspective considering water consumption, energy consumption, GHG emissions, and internal costs. J. Environ. Manag. 255, 109860. https://doi.org/10.1016/j.jenvman.2019.109860.

Mao, C., Qu, Q., Li, F., Fang, C., Li, H., Ding, J., Wan, H., Zhang, P., Guan, G., 2024. Nickel phosphide cocatalyst and carbon defects simultaneously boosting the photocatalytic hydrogen production over carbon nitride. J. Environ. Chem. Eng. 12, 112271. https://doi.org/10.1016/j.jece.2024.112271.

Mele, M.A., Kumar, R., Dada, T.K., Heydari, A., Antunes, E., 2024. Investigation of gold adsorption by ironbark biochar using response surface methodology and artificial neural network modelling. J. Clean. Prod. 456, 142317. https://doi.org/10.1016/j.jclepro.2024.142317.

Minaei, S., Benis, K.Z., McPhedran, K.N., Soltan, J., 2024. Adsorption of sulfamethoxazole and lincomycin from single and binary aqueous systems using acid-modified biochar from activated sludge biomass. J. Environ. Manag. 358, 120742. https://doi.org/10.1016/j.jenvman.2024.120742.

Padilla, E.R.D., Hansted, F.A.S., Luna, C.M.R., Campos, C.I., Yamaji, F.M., 2024. Biochar derived from agricultural waste and its application as energy source in blast furnace. Renew. Energ. 220, 119688. https://doi.org/10.1016/j.renene.2023.119688.

Popat, P.R., Alyami, A.Y., Inwati, G.K., Makwana, B.A., Alreshidi, M.A., Algethami, J.S., Abbas, M., Yadav, K.K., 2024. Enriched adsorption of methyl orange by zinc doped lithium manganese oxides nanosorbent. Inorg. Chem. Commun. 161, 112016. https://doi.org/10.1016/j.inoche.2023.112016.

Shi, G., Liu, H., Chen, H., Liu, T., Liang, D., Hua, X., Dong, D., 2024. Nitrogen self-doped Chlorella biochar as a peroxydisulfate activator for sulfamethazine degradation: the dominant role of electron transfer. J. Clean. Prod. 440, 140951. https://doi.org/10.1016/j.jclepro.2024.140951.

Singh, B.K., Mercier-Bion, F., Lefevre, G., Simoni, E., 2016. Effect of short chain aliphatic carboxylic acids for sorption of uranyl on rutile Zeta potential and in situ ATR-FTIR studies. J. Ind. Eng. Chem. 35, 325–331. https://doi.org/10.1016/j.jiec.2016.01.008.

Son, J.Y., Choe, S., Jang, Y.J., Kim, H., 2024. Waste paper-derived porous carbon via microwave-assisted activation for energy storage and water purification. Chemosphere 355, 141798. https://doi.org/10.1016/j.chemosphere.2024.141798.

Su, J., Zhang, M., Xu, W., Xu, W., Liu, C., Rui, S., Tuo, Y., He, X., Xiang, P., 2024. Preparation and applications of iron/biochar composites in remediation of heavy metal contaminated soils: current status and further perspectives. Environ. Technol. Innov. 35, 103671. https://doi.org/10.1016/j.eti.2024.103671.

Teather, R.M., Wood, P.J., 1982. Use of Congo red-polysaccharide interactions in enumeration and characterization of cellulolytic bacteria from the bovine rumen. Appl. Environ. Microb. 43. https://doi.org/10.1128/aem.43.4.777-780.1982.

Wang, Z., Li, J., Yang, H., Su, X., Bushra, R., Guo, J., Zhu, W., Khan, M.R., Xiao, H., Song, J., 2024. Enhancing the mechanical strength of corrugated medium paper through instant catapult steam explosion pretreatment of tobacco stem. Ind. Crop. Prod. 218, 119005. https://doi.org/10.1016/j.indcrop.2024.119005.

Wen, C., Liu, T., Wang, D., Wang, Y., Chen, H., Luo, G., Zhou, Z., Li, C., Xu, M., 2023. Biochar as the effective adsorbent to combustion gaseous pollutants: preparation, activation, functionalization and the adsorption mechanisms. Prog. Energ. Combust. 99, 101098. https://doi.org/10.1016/j.pecs.2023.101098.

Yang, D., Deng, R., Chen, M., Liu, T., Luo, L., He, Q., Chen, Y., 2023. Biochar-based microporous nanosheets-mediated nanoconfinement for high-efficiency reduction of Cr(VI). J. Hazard. Mater. 459, 132283. https://doi.org/10.1016/j.jhazmat.2023.132283.

Yu, S., Zhang, W., Dong, X., Wang, F., Yang, W., Liu, C., Chen, D., 2024. A review on recent advances of biochar from agricultural and forestry wastes: preparation, modification and applications in wastewater treatment. J. Environ. Chem. Eng. 12, 111638. https://doi.org/10.1016/j.jece.2023.111638.

Zarrik, B., Amri, A.E., Bensalah, J., Jebli, A., Lebkiri, A., Hbaiz, R.E.M., Rifi, E.H., Lebkiri, A., 2024. Adsorption of crystal violet using a composite based on graphene Oxide-ED@Cellulose: adsorption modeling, optimization and recycling. Inorg. Chem. Commun. 162, 112179. https://doi.org/10.1016/j.inoche.2024.112179.

Zhang, J., Li, Q., Zhang, J., Liu, H., Wang, H., Zhang, J., 2025. Enhanced CO_2 absorption in amine-based carbon capture aided by coconut shell-derived nitrogen-doped biochar. Sep. Purif. Technol. 353, 128451. https://doi.org/10.1016/j.seppur.2024.128451.

Zhu, Z., Yang, X., Ye, X., Li, Q., Wang, J., Wu, L., Huang, Z., Wang, M., 2024. Activating peroxymonosulfate by high nitrogen-doped biochar from lotus pollen for efficient degradation of organic pollutants from water: performance, kinetics and mechanism investigation. Sep. Purif. Technol. 346, 127456. https://doi.org/10.1016/j.seppur.2024.127456.